AIAA AVIATION Forum
12-16 June 2023, San Diego, CA and Online
AIAA AVIATION 2023 Forum

10.2514/6.2023-4188

Turbulence interaction noise from a rectilinear cascade of airfoils and effects of porous material inclusions

Vincent Clair*, Edouard Salze †, Pascal Souchotte ‡ and Emmanuel Jondeau §
Univ Lyon, École Centrale de Lyon, INSA Lyon, Université Claude Bernard Lyon I, CNRS, Laboratoire de Mécanique des Fluides et d'Acoustique, UMR 5509, 36 Avenue Guy de Collongue, F-69134, Ecully, France

The broadband noise radiated by turbulent fan wakes interacting with the outlet guide vanes is one of the major broadband noise components of turbofan engines. In this paper, this broadband turbulence interaction noise is studied experimentally in an anechoic wind tunnel on a simplified configuration consisting in a rectilinear cascade of airfoils impinged by a turbulent flow generated by a turbulence grid. The cascade is made of 7 loaded airfoils with an adjustable incidence angle and the upstream flow velocities investigated are up to a Mach number of 0.53. The noise radiated by the cascade is evaluated using a circular array of microphones located in free-field downstream of the cascade, and also using a linear array of microphones flush mounted in the duct upstream of the cascade. A concept of airfoil with inclusions of porous material has been designed based on previous work and manufactured to be tested on this rectilinear cascade configuration. The results of the measurements performed with this airfoil concept are compared to the results of the fully rigid reference airfoil.

Downloaded by Christophe Bogey on October 11, 2023 | http://arc.aiaa.org | DOI: 10.2514/6.2023-4188

I. Introduction

Aircraft noise is a major source of nuisance for the communities living in the vicinity of airports. As the noise radiated from the engines is one of the main contributors to aircraft noise during the approach and take-off phases, its reduction is a major concern for engine manufacturers in order to comply with future regulations and guideline, such as the ACARE flight path 2050. Modern turbofan engines architectures known as Ultra-High Bypass Ratio (UHBR) engines aim at improving the engine efficiency by increasing the bypass ratio, using a larger fan with a lower rotational velocity. For such architectures, the fan-Outlet Guide Vanes (OGV) stage is one of the main source of engine noise, especially at approach conditions [1, 2]. Typical fan-OGV noise consists in a tonal component at multiples of the Blade Passing Frequency (BPF) and a broadband component. The tonal component is mostly associated with the highly coherent wakes developing downstream of the fan and impinging on the OGV. This contribution has been widely studied in the literature and a number of solutions have been proposed and applied over the past decades [1]. For example, the number of fan blades and outlet guide vanes can be chosen to take advantage of duct propagation effects and ensure that the BPF is cut-off [3]. Acoustic liners are now commonly used in the casing of engines to damp tonal components as well [4]. The broadband component of fan-OGV noise is a more recent concern that emerged with the reduction of the tonal components and the move towards larger fan diameters. Broadband noise is associated with the finer and less coherent turbulent structures present in the boundary layers and in the wakes of the fan. The main broadband noise generation mechanism is known as turbulence interaction noise and is due to the turbulent structures of the fan's wake impinging on the OGV. Because of its wide frequency range and very rich modal content, some of the noise reduction solutions designed for tonal noise are much less efficient on broadband noise.

In the past decade, passive solutions were imagined and investigated to reduce this broadband component of the turbulence interaction noise. A first set of solutions, often referred to as serrations, consists in modifying the shape of the leading edge by introducing periodic patterns in the spanwise direction. The acoustic performances of serrations have been widely investigated, mostly on single airfoil configurations. Sinusoidal serrations are the most commonly studied [5–9], but other shapes such as the superposition of two sine curves [10] and a sawtooth pattern with or without slits [11] were also considered. These concepts showed promising performances, provided that the parameters defining the leading edge shape (pattern wavelength, serration depth) are carefully chosen with regards to the characteristic length of the incident turbulence.

*Assistant Professor, vincent.clair@ec-lyon.fr
†Research Engineer
‡Research Engineer
§Research Engineer

Copyright © 2023 by Vincent Clair, Edouard Salze, Pascal Souchotte and Emmanuel Jondeau.
Published by the American Institute of Aeronautics and Astronautics, Inc., with permission.

Another kind of passive solutions that were investigated rely on the use of porous material on the OGV. Some of the work was dedicated to trailing edge noise [12, 13] which is not the noise source of interest in the present paper. The use of porous material on airfoils was also considered as a way to reduce turbulence interaction noise and tested on single airfoils at relatively low flow velocities [6, 8, 14]. Broadband noise reductions were observed, but the impact of such a concept on the aerodynamic performances of the airfoils remains to be assessed, particularly for loaded airfoils at higher flow velocities.

Turbulence interaction noise received a lot of experimental, numerical and analytical attention on single airfoil setups, especially for the assessment of noise reduction concepts. Analytical techniques have been developed to estimate the acoustic response of airfoil cascades [15–20] impinged by turbulent flows, usually considering that the airfoils can be assimilated to flat plates with no thickness. Some work is ongoing to account for the camber of the airfoils [21, 22]. Experimentally, turbulence interaction noise on airfoil cascades configurations has received limited attention. A very early study took interest in the aerodynamic and acoustic performances of airfoils in a rectilinear cascade configuration, including the effects of leading edge serrations [23]. More recent experimental work has been carried out in anechoic wind tunnels to investigate turbulence interaction noise radiated by a rectilinear cascade of airfoils [24], an annular cascade of OGV [25], and a rectilinear cascade of flat plates with leading edge serrations [26]. These studies were carried out at low to moderate flow speed.

The present paper is dedicated to an experimental study of the broadband noise radiated by a rectilinear cascade of airfoils impinged by grid generated turbulence, for flow velocities up to a Mach number M = 0.53. This test campaign took place within the framework of the European project InnoSTAT, aiming at developing and assessing broadband noise reduction concepts applied to OGVs in order to increase their Technology Readiness Level. Within this project, a concept of OGV with inclusions of porous materials was developed based on previous work [6, 8, 14] and tested. The experimental setup of the test campaign, and the design of the airfoil with porous inclusions is presented in section II of this paper. The aerodynamic and acoustic results are then presented for the cascade nominal frontline angle in section III.

II. Experimental setup

A. Test rig

The experimental campaign took place in LMFA's anechoic open jet wind tunnel at Ecole Centrale de Lyon, shown in figure 1. The airflow is generated by a centrifugal fan powered by an 800 kW engine, with a maximum mass flow rate of about 20 kg/s, and passes through a series of acoustic treatments before entering the 720 m^3 anechoic room through a 0.56×0.56 m^2 section.

Fig. 1 Anechoic wind tunnel at Ecole Centrale de Lyon.

The cascade is composed of 7 NACA 7310 airfoils with a chord $c = 0.12$ m, a span $L = 0.2$ m and an inter-vane spacing $s = 0.085$ m. One of the objectives of this experimental campaign is to perform acoustic measurements of the noise radiated by the cascade for flow velocities up to a Mach number of M = 0.53. A dedicated test section has been designed to install the airfoil cascade (see figure 2). A 0.5 m long nozzle adapts the test section from 0.56×0.56 m^2 to

Downloaded by Christophe Bogey on October 11, 2023 | http://arc.aiaa.org | DOI: 10.2514/6.2023-4188

0.56×0.2 m^2. A turbulence grid can be inserted just upstream of the nozzle. The leading edge of the central airfoil is located at about 0.5 m downstream of the nozzle. The vertical side plates downstream of the nozzle are guiding the flow down to the trailing edge of the cascade, while the horizontal plates extend downstream of the cascade as semicircles centered on the trailing edge of the central airfoil. Brushes have been attached to the horizontal plates, as visible in figure 2 (right), to limit the presence of additional acoustic sources. The airfoils are mounted inbetween two large disks embedded in the horizontal plates, which allows the rotation of the cascade around the trailing edge of the central airfoil. Thus, the angle β_c between the incident flow and the normal to the cascade frontline, as defined in figure 3 (left), can be adjusted. In this experimental campaign, the stagger angle is kept constant at a value $\chi = 13°$. Thus, variations in the cascade frontline angle β_c correspond to variations of the incidence angle of the airfoils α_c. The nominal value of the cascade frontline angle is $\beta_c = 34°$ and it can vary in the range $\beta_c = 34 \pm 8°$. The nominal and extreme angular positions of the airfoils are shown in figure 3 (right). Note that, because the flow is deflected by the airfoil cascade, a bend is located upstream of the nozzle (see figure 2) to ensure that the flow downstream of the cascade exits the anechoic room through the dedicated opening and does not impinge on the acoustic treatments of the room. A set of deflector plates is installed in this bend to allow for the flow rotation without separation.

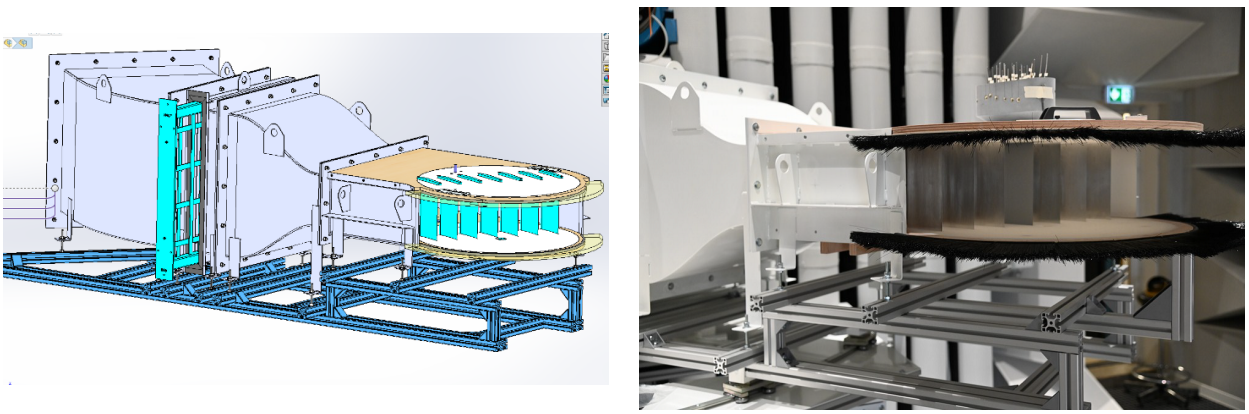

Fig. 2 Test section designed for the experimental campaign.

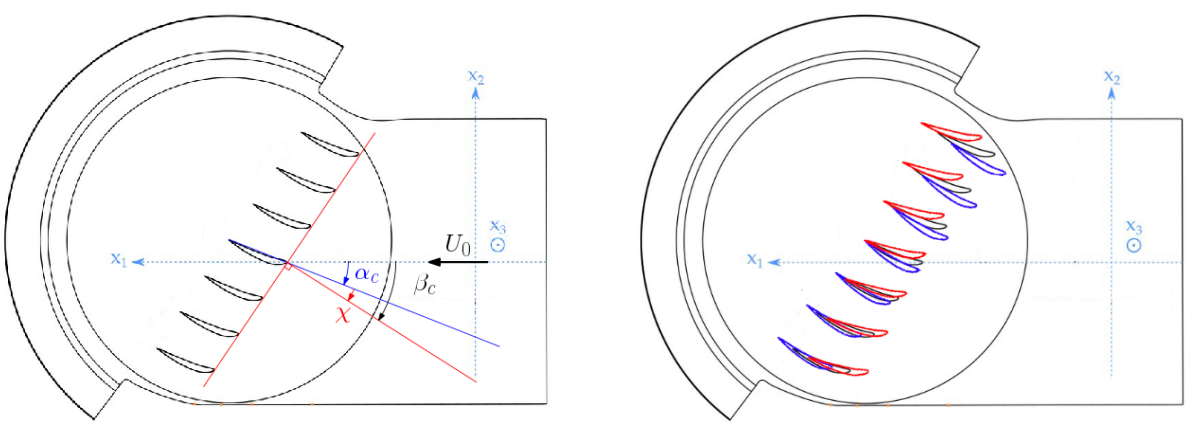

Fig. 3 Definitions of the stagger angle χ, the incidence angle α_c and the cascade front angle β_c (left). Positions of the airfoils for values of the β_c angle $\pm 8°$ around its nominal value.

B. Instrumentation

Aerodynamic measurements are realized upstream of the cascade to check the homogeneity of the flow through the test section, and to characterize the turbulent flow generated by the turbulence grid. The locations of these measurements

Downloaded by Christophe Bogey on October 11, 2023 | http://arc.aiaa.org | DOI: 10.2514/6.2023-4188

is presented in figure 4 (left). The green line corresponds to a set of 35 static pressure probes, flush mounted on the lower horizontal plate of the test section to assess the homogeneity of the flow in the transverse direction (notably to check that there is no separation because of the bend installed upstream of the test section). The red lines and dots correspond to hot-wire measurements. Velocity profiles are measured in the mid-span plane over lines parallel to the cascade front line located 0.2 m and 0.05 m upstream of the cascade. These profiles are measured both with a single component hot-wire probe and with a two component cross wire probe, shown in figure 4 (bottom, right). Boundary layer velocity measurements are also performed over the lower horizontal plate with a hot-wire probe just downstream of the nozzle, as visible in figure 4 (top, right). Additionally, velocity profiles are also measured in the wake of the airfoil, 0.015 m downstream of the trailing edges, with a single component hot-wire probe. These wake profiles are only measured for the nominal value of the cascade frontline angle $\beta_c = 34°$.

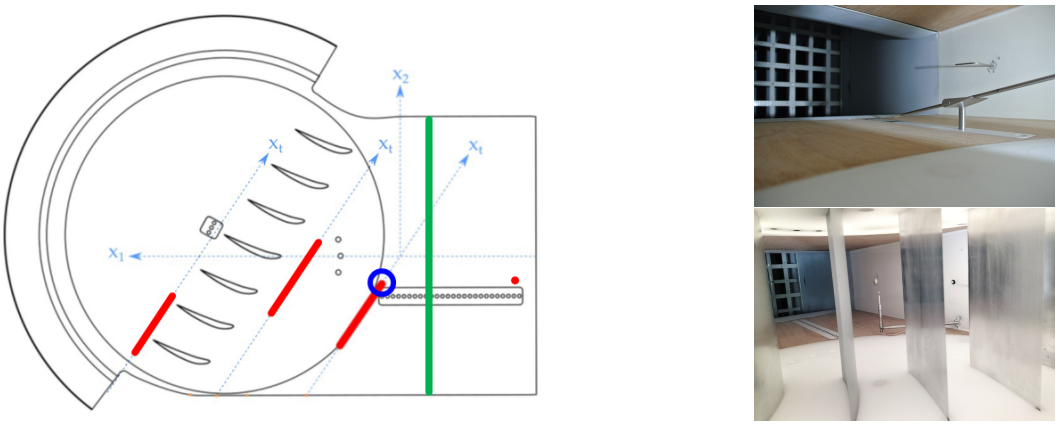

Fig. 4 Positions of the static pressure probes in green and of the hot-wire measurements in red (left). Picture of the hot-wire probes used for the boundary layer measurements (right, top). Picture of the X wire probe used for the 2 components velocity measurements (right, bottom).

Acoustic measurements are performed both upstream and downstream of the cascade. The positions of the microphones are shown in figure 5 (left), and the microphones installed upstream of the cascade can also be seen in figure 4 (left).

A linear array comprising 26 microphones is installed upstream of the cascade. The microphones are flush mounted and the array can be used to separate the acoustic waves propagating in the upstream direction (radiated by the airfoil cascade) from the perturbations propagating in the downstream direction, either acoustic waves or hydrodynamic wall pressure fluctuations.

Three microphones are located just downstream of the trailing edge of the central airfoil, and a circular array of 14 microphones is located downstream of the cascade, in the far-field. This circular array is centered around the trailing edge of the central airfoil and has a radius of $R = 1.95$ m. The microphones are positioned in the mid-span plane, with an angular spacing of 10° from $\theta = -90°$ to $\theta = +90°$ with regards to the downstream flow direction. No microphones are installed in the flow downstream of the cascade at angles between $\theta = -20°$ to $\theta = +40°$.

Additionally, for the reference configuration (rigid airfoils), the central airfoil is equipped with 24 pinholes connected to tubes that allow to perform both static pressure measurements and fluctuating pressure measurements using remote microphones and a dedicated calibration procedure. The positions of the pinholes on the surface of the airfoil is shown in figure 5 (right).

C. Airfoil with porous inclusions design

The concept tested in this experimental campaign relies on previous work by Bampanis [8] and Bampanis & Roger [14] on a single airfoil configuration at low flow velocities. In their work, the design consisted in a rigid centerplate with stiffeners following the shape of the targeted airfoil geometry. The space between the chordwise and spanwise stiffeners was filled with a porous material (melamine foam or metal wool) and a wiremesh was attached to the stiffeners to form the surface of the airfoil.

The noise reduction effects were expected to be associated with two mechanisms. The first one is an attenuation of

Downloaded by Christophe Bogey on October 11, 2023 | http://arc.aiaa.org | DOI: 10.2514/6.2023-4188

Downloaded by Christophe Bogey on October 11, 2023 | http://arc.aiaa.org | DOI: 10.2514/6.2023-4188

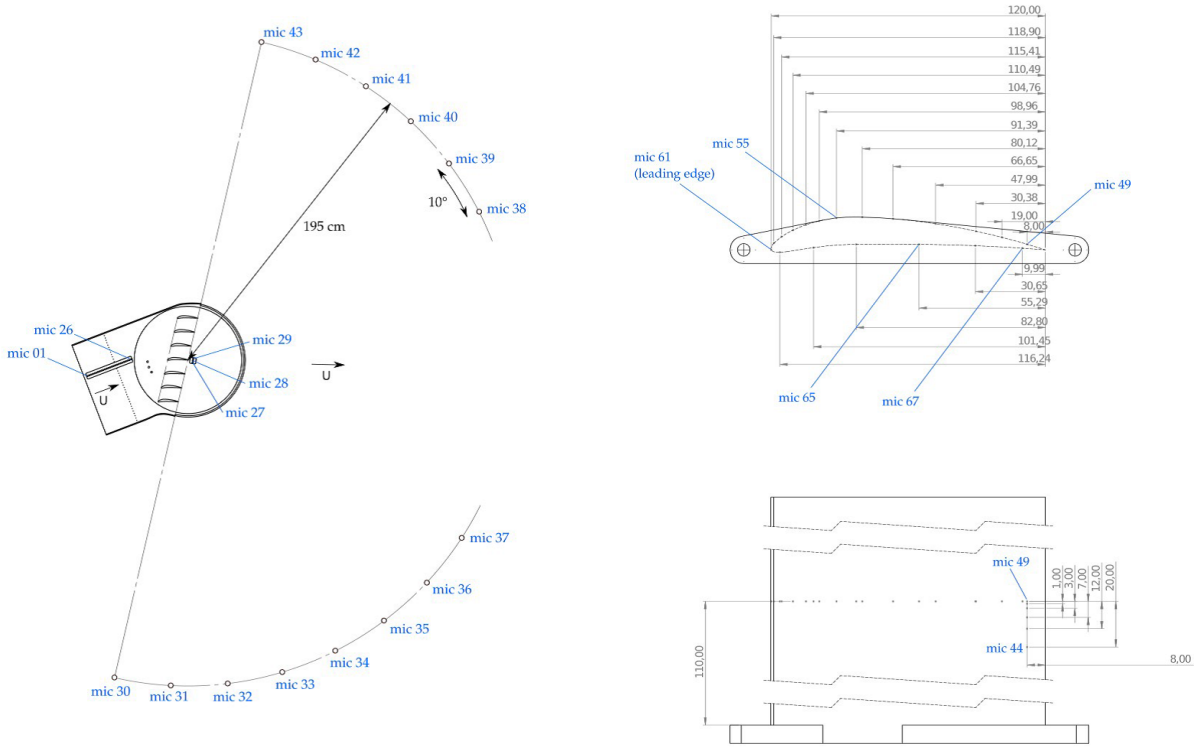

Fig. 5 Positions of the microphones in the test section and on the far-field array (left). Positions of the pinholes used for static pressure and fluctuating pressure measurements on the surface of the central vane for the reference geometry (right).

the impingement of turbulent structures in the leading edge region, which is the source of turbulence interaction noise. The second effect is related to the propagation of the acoustic waves radiated from the leading edge along the airfoil, acting as an acoustic liner.

The airfoil considered was symmetric (NACA 0012), and it was tested at a 0° angle of attack, thus with no mean loading. The possibility to leave a gap between the leading edge and the rigid centerplate was investigated and showed to improve the acoustic performances of the airfoil. A drawback of this idea is that, for a loaded airfoil, some flow would go through the airfoil in the gap and deteriorate the aerodynamic performances of the airfoil. The main difficulty encountered in this previous work is associated with the wiremesh being attached only to the stiffeners to form the surface of the airfoil. Even at low flow flow velocities, it was observed that the wiremesh would deform, and thus not preserve the airfoil shape. This is expected to be even more problematic for higher flow velocities and for loaded airfoils.

In the present experiments, the flow velocity is up to M = 0.53 and the airfoils of the cascade are highly loaded. Thus, the solution previously investigated by Bampanis & Roger had to be adapted to provide more rigidity to the surface of the airfoil and prevent deformation. The design still relies on a rigid frame, consisting in a centerplate that follow the camber line of the airfoil and stiffeners in the streamwise and spanwise direction. In the trailing edge region, because of the limited thickness available, the airfoil is fully rigid. A view of this rigid frame is visible in figure 6 (left). The spaces between the stiffeners is filled with melamine foam. Note that, because of the overall thickness of the airfoil, the maximum thickness of melamine foam on each side of the airfoil is about 5 mm. In order to provide a more rigid layer at the surface of the airfoil, a perforated plate with square perforations is bent to the shape of the airfoil and welded on top of the rigid frame. This grid also provides for more surface to glue the wiremesh on top of it. The final assembly can be seen in figure 6 (right), where the outline of the grid is visible under the wiremesh.

In terms of the noise reduction effects described above, the addition of the grid reduces the porosity of the surface and might thus lead to a reduced efficiency. However, as the airfoils will be installed in a cascade configuration, the absorption of acoustic waves propagating between the airfoils might be improved compared to a single airfoil

configuration.

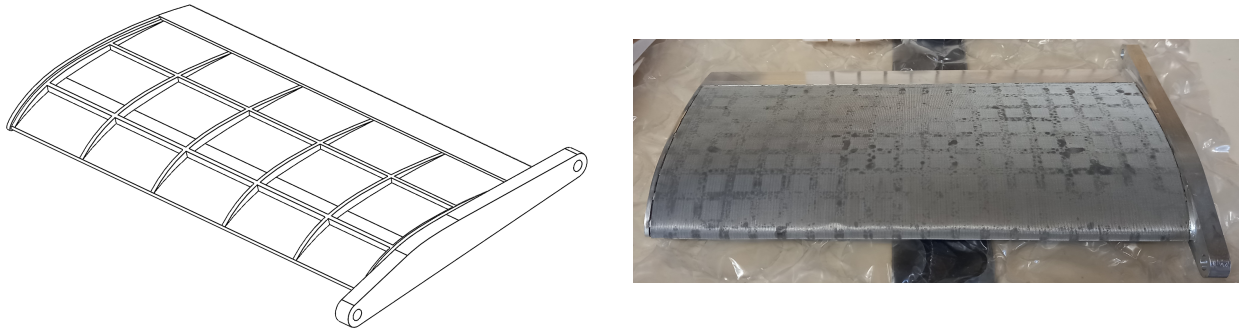

Fig. 6 Airfoil with porous inclusions. CAD view of the rigid centerplate and stiffeners (left), and picture of an assembled airfoil (right).

Downloaded by Christophe Bogey on October 11, 2023 | http://arc.aiaa.org | DOI: 10.2514/6.2023-4188

III. Results at the nominal cascade frontline angle

In this section, the results are presented for the nominal value of the cascade frontline angle $\beta_c = 34°$. The trends observed at other values of β_c considered in the test campaign do not differ significantly.

A. Upstream flow characteristics

The flow is first investigated upstream of the cascade to assess its homogeneity through the test section. The velocity spectrum of the turbulence generated by the turbulence grid located upstream of the nozzle is also characterized, as it is the main parameter of the turbulence interaction noise mechanism, which is the source of interest in this work.

Figure 7 shows the static pressure profiles measured in the transverse direction along the lower horizontal plate, upstream of the airfoil cascade (but downstream of the nozzle). These results show a uniform distribution of static pressure across the section which is indicative that the flow does not display any region of separation due to the presence of the bend upstream of the nozzle.

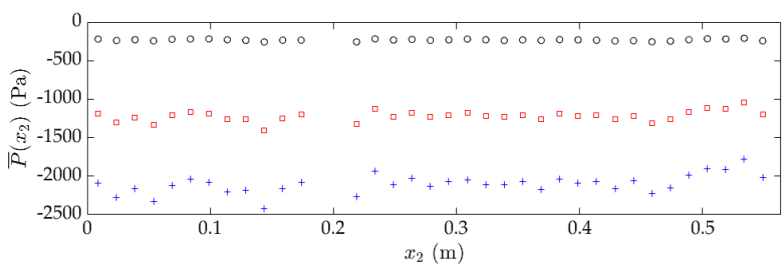

Fig. 7 Transverse profiles of the static pressure upstream of the cascade for the upstream flow velocities: 45 m/s (black), 75 m/s (red) and 100 m/s (blue).

Figure 8 presents the mean velocity profiles measured with a single component hot-wire probe along a line parallel to the cascade frontline, located 0.2 m upstream of the airfoil leading edges. The position of this profile is visible in figure 4 (left) in red. The mean velocity profiles are normalized by the average value calculated over the whole profile. For the two flow velocities presented, only a ±1% deviation from the averaged value is visible. These profiles were measured without the turbulence grid and it was observed that the distance between the velocity deficits corresponds to the distance between the deflector plates located in the bend upstream of the nozzle.

The turbulent velocity spectra calculated from single hot-wire measurements at the position circled in blue in figure 4 (left) are presented in figure 9 in black lines for two flow velocities. These experimental spectra can be used to estimate an integral length scale Λ and the turbulent intensity T_I of the turbulence impinging on the cascade.

The turbulent intensity is defined as $T_I = \sqrt{\overline{u'^2}}/U_0^2$, where U_0 is the mean value of the flow velocity and $\overline{u'^2}$ is the

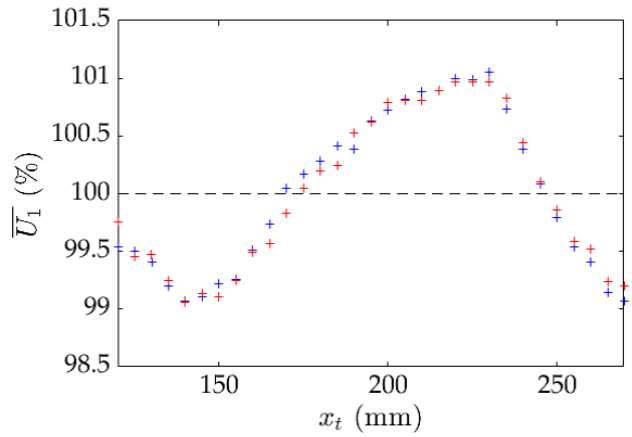

Fig. 8 Normalized mean velocity profiles 0.2 m upstream of the cascade, measured without the turbulence grid, for the upstream flow velocities: 45 m/s (blue) and 100 m/s (red).

mean square value of the velocity fluctuation component measured by the hot-wire probe. The latter can be calculated from the experimental one-sided frequency spectra showed in figure 9:

$$\overline{u'^2} = \int_0^{+\infty} S_{uu}(f)\ \mathrm{d}f \tag{1}$$

where S_{uu} is the velocity spectrum.

The integral length scale can be calculated as:

$$\Lambda = \frac{U_0 S_{uu}(f=0)}{4\overline{u'^2}} \tag{2}$$

In practice, an average of the experimental spectra over the first 10 points is used instead of $S_{uu}(f=0)$.

These values of $\overline{u'^2}$ and Λ can then be used in a standard homogeneous and isotropic turbulent velocity spectrum model such as the Liepmann model to assess its adequacy with the experimental results. It is also possible to assume a turbulence model (here the Liepmann spectrum) and perform a least square fit of the model to the experimental data to deduce values for $\overline{u'^2}$ and Λ.

The expression the one-sided frequency spectrum of the axial velocity fluctuation for the Liepmann model is:

$$S_{uu}(f) = \frac{4\overline{u'^2}\Lambda}{U_0}\frac{1}{1+k_1^2\Lambda^2} \tag{3}$$

with $k_1 = 2\pi f/U_0$.

In figure 9, the Liepmann spectra calculated using the theoretical values of $\overline{u'^2}$ and Λ as defined in equations (1) and (2) are shown in blue lines, and the Liepmann spectra deduced from a least square fit are shown in red lines. It can be seen that both the theoretical spectrum and least square fit match very well with the experimental data. Only a slight vertical shift can be observed between the two Liepmann spectra at $U_0 = 43$ m/s. The values of T_I and Λ deduced from equations (1) and (2), as well as from the least square fit of a Liepmann model are presented in table 1. The two set of values are very close to one another. It can be noted that the values of T_I and Λ are evolving slightly between the two flow velocities presented.

B. Wake profiles

Velocity measurements have been performed in the wake of the cascade using a single component hot-wire probe, 15 mm downstream of the trailing edges along a line represented in red in figure 4 (left). The velocity profiles (mean and RMS values) are normalized by the mean velocity measured in the middle of a cascade channel (between two airfoils).

The mean velocity wake profiles are presented in figure 10 for two flow velocities. For the porous configuration, the maximum velocity deficit is significantely larger than for the reference, and the wake is much wider. The widening of

Downloaded by Christophe Bogey on October 11, 2023 | http://arc.aiaa.org | DOI: 10.2514/6.2023-4188

Downloaded by Christophe Bogey on October 11, 2023 | http://arc.aiaa.org | DOI: 10.2514/6.2023-4188

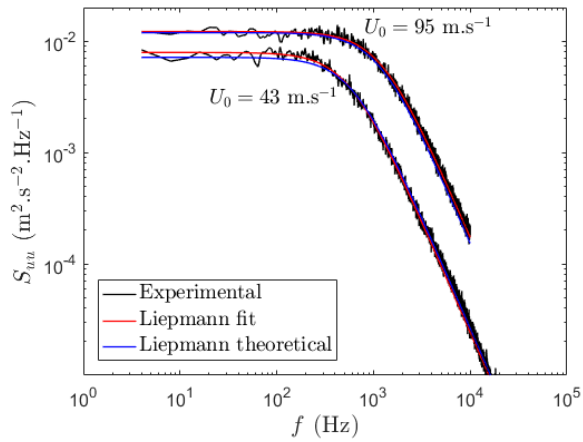

Fig. 9 Turbulent velocity spectrum of the axial velocity component measured 0.2 m upstream of the cascade.

	U_0 = 43 m/s		U_0 = 95 m/s	
	T_I (%)	Λ (mm)	T_I (%)	Λ (mm)
Theoretical	6.1	11.2	4.9	13.3
Liepmann least square fit	6.5	11.2	5.0	12.6

Table 1 Values of the turbulence intensity and the integral length scale deduced from the experimental velocity spectra.

the wake appears even more important for the highest velocity. The position of the wake is shifted towards the suction side for the porous configuration. Overall, these wakes may be indicative of a flow separation on the suction side, or at least an important thickening of the boundary layers, and lead to a deterioration of the aerodynamic performances for the porous configuration.

The profiles of the RMS value of the velocity fluctuations measured in the wake are shown in figure 11. The amplitude and width of the velocity fluctuation are increased for the porous case, particularly at the highest velocity. The trace of the boundary layers forming on both sides of the airfoil are visible on these profiles. It appears that the thickness of the boundary layer on the suction side has increased a lot for the porous airfoil, which is consistent with the hypothesis of a flow separation.

It is unclear if this supposed separation is associated with the behavior of the flow along the airfoil, as the fluid may flow through the porous surface and interact with the stiffeners, or if it associated to a difference in the geometry of the airfoil compared to the reference because of its complex assembly.

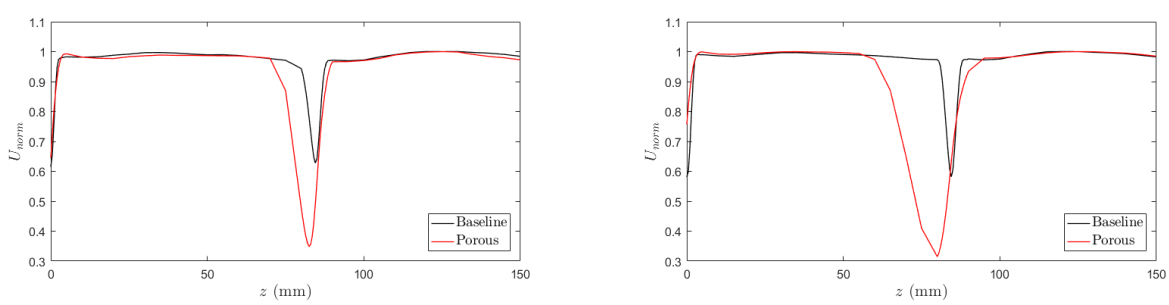

Fig. 10 Mean velocity profiles measured downstream of the airfoils, normalized by the mean velocity in the middle of a cascade channel. The cascade frontline angle is $\beta_c = 34°$ and the upstream flow has a velocity $U_0 = 46$ m/s (left) and $U_0 = 100$ m/s (right).

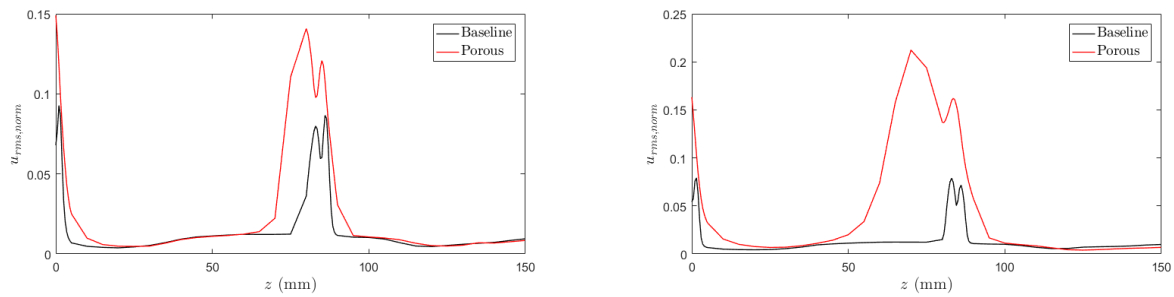

Fig. 11 RMS velocity profiles measured downstream of the airfoils, normalized by the mean velocity in the middle of a cascade channel. The cascade frontline angle is $\beta_c = 34°$ and the upstream flow has a velocity $U_0 = 46$ m/s (left) and $U_0 = 100$ m/s (right).

C. Acoustic results

In this section, the acoustic results will be presented for two upstream flow velocities corresponding to Mach numbers M = 0.34 and M = 0.53.

First, the Power Spectral Density (PSD) of the pressure fluctuation measured by the microphone located at $\theta = -60°$ on the downstream circular array are presented in figure 12. The reference pressure used for the dB scale is $p_{ref} = 2 \times 10^{-5}$ Pa. For the two flow velocities considered, it appears that the use of porous airfoils leads to an increase of the noise up to 2-2.5 kHz. This increase is particularly visible from 1 kHz to 2.5 kHz. At higher frequencies, a reduction of the noise is observed consistently up to at least 10 kHz. Since the most energetic part of these spectra is located below 2 to 3 kHz, this would indicate that the overall performances of the porous airfoils may not be positive in terms of noise reduction.

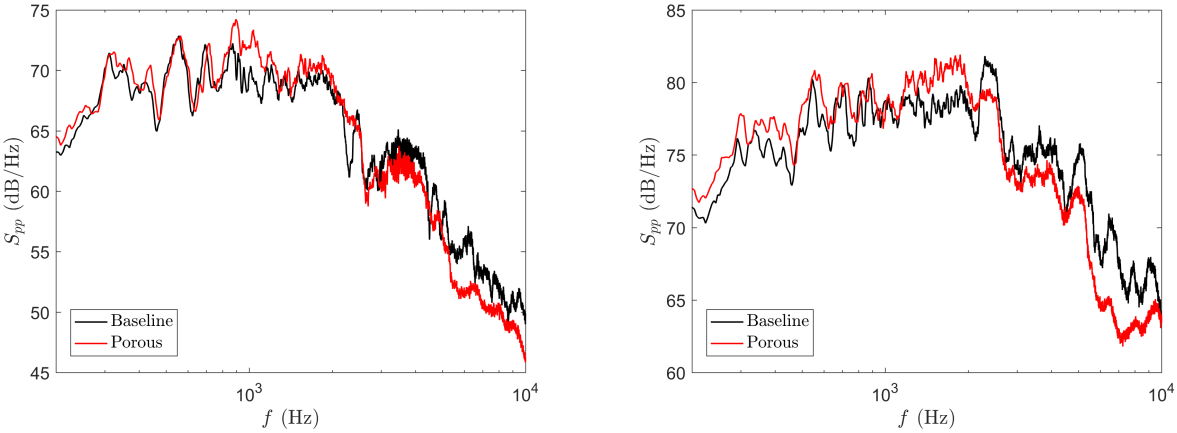

Fig. 12 Power Spectral Density of the pressure fluctuation measured on the downstream circular array at $\theta = -60°$ (microphone 33). The cascade frontline angle is $\beta_c = 34°$ and the upstream flow has a Mach number M = 0.34 **(left) and** M = 0.53 **(right).**

The Overall Sound Pressure Levels (OASPL), integrated between 200 Hz and 10 kHz, measured over the downstream circular array are shown in figure 13. These confirm that, over this whole frequency range, the porous airfoils do not seem to perform very well. A small but consistent increase in OASPL of about 1 dB can be seen at M = 0.34. For M = 0.53, the OASPL of the reference and porous configurations show very similar results, with a small but almost insignificant noise reduction at some angles for the porous configuration.

Using the microphone measurements over the downstream circular array, the acoustic power radiated by the cascade in the downstream direction can be estimated, assuming that the radiation from the cascade behaves as spherical waves in the far-field. Thus, the acoustic power radiated through a surface S can be calculated by:

Downloaded by Christophe Bogey on October 11, 2023 | http://arc.aiaa.org | DOI: 10.2514/6.2023-4188

Downloaded by Christophe Bogey on October 11, 2023 | http://arc.aiaa.org | DOI: 10.2514/6.2023-4188

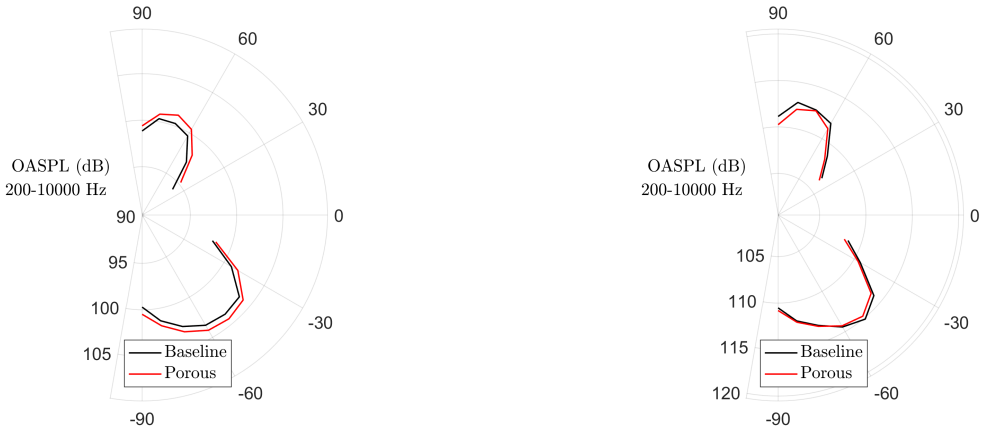

Fig. 13 Overall Sound Pressure Level, integrated between 200 Hz and 10 kHz, measured on the downstream circular array. The cascade frontline angle is $\beta_c = 34°$ and the upstream flow has a Mach number M = 0.34 **(left) and** M = 0.53 **(right).**

$$W(f) = \int_S \frac{S_{pp}(f)}{\rho_0 c_0} \, \mathrm{d}S \tag{4}$$

where S_{pp} is the power spectral density of the pressure fluctuation, ρ_0 the mean density and c_0 the speed of sound at the microphone positions. Here, since the microphones of the circular array have an angular spacing $\Delta\theta = 10°$, the surface element used for each microphone to approximate the integral in equation (4) corresponds to a sphere surface element with $R = 1.95$ m and $\Delta\theta = \Delta\varphi = 10°$.

The acoustic power in dB is then defined as:

$$PWL(f) = 10 \log_{10} \left(\frac{W(f)}{W_{ref}} \right) \tag{5}$$

with $W_{ref} = 1 \times 10^{-12}$ W.

The downstream acoustic power spectra are presented in figure 14. They show trends that are quite similar to the PSD shown in figure 12, with an increase of the noise radiated below 2-2.5 kHz (especially from 1 kHz to 2.5 kHz), and a noise reduction at higher frequencies.

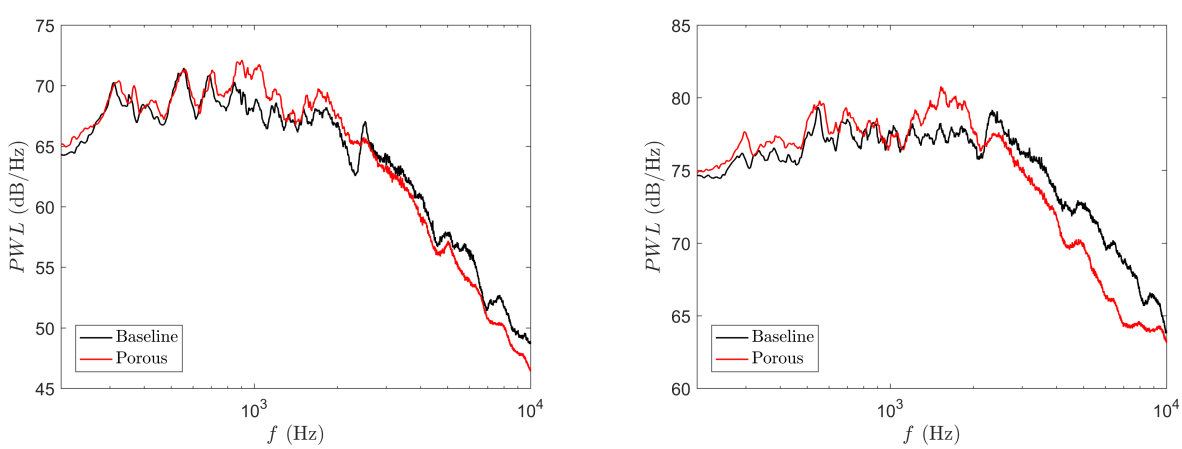

Fig. 14 Acoustic power spectra integrated over the downstream circular array. The cascade frontline angle is $\beta_c = 34°$ and the upstream flow has a Mach number M = 0.34 **(left) and** M = 0.53 **(right).**

Upstream of the cascade, in the duct, the pressure signals recorded by a flush mounted microphone alone would not be indicative of the noise radiated by the airfoil cascade, as these signals also contain the wall pressure fluctuations of the turbulent boundary layer developing along the plate. Thus, as mentioned in section II.B, the duct section upstream of the cascade is equipped with a linear array of microphones flush mounted on the lower horizontal plate and aligned in the axial direction. This array can be used to separate the acoustic waves propagating upstream (radiated by the airfoil cascade) from the perturbations traveling in the downstream direction, such as the wall pressure fluctuations of the turbulent boundary layer, as depicted in figure 15.

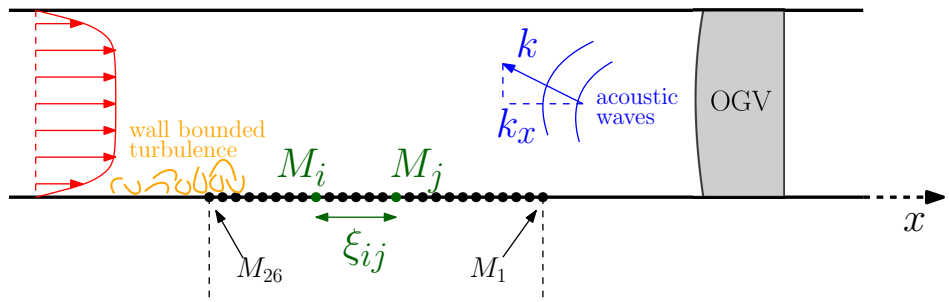

Fig. 15 Schematic of the upstream linear microphone array, and of the upstream and downstream propagating pressure perturbations.

To do so, the cross-spectral matrix S_{ij} is formed from the Fourier transforms of the pressure signals $\hat{p}$, for each pair of microphones (i, j), using a periodogram method with N segments of duration T:

$$\begin{aligned} S_{ij}(\xi_{ij}, \omega) &= \frac{2\pi}{T}\frac{1}{N}\sum_{n=1}^{N} \hat{p}_n(x_i, \omega)\hat{p}_n^*(x_j, \omega) \\ &= \frac{2\pi}{T}\frac{1}{N}\sum_{n=1}^{N} \hat{p}_n(x_i, \omega)\hat{p}_n^*(x_i + \xi_{ij}, \omega) \end{aligned} \tag{6}$$

where $\xi_{ij} = x_j - x_i$ is the separation between the microphones i and j. The elements of S_{ij} are then ranked by increasing value of ξ_{ij} and, when several pairs of microphones have the same value of ξ_{ij}, only one pair is kept. This results in an array $S(\xi, \omega)$ containing a cross-spectrum for each value of the separation ξ that can be obtained with the microphone array.

The wavenumber-frequency spectrum is then defined by:

$$\Phi_{pp}(k_x, \omega) = \frac{1}{2\pi}\int_{-\infty}^{\infty} S(\xi, \omega)\mathrm{e}^{-\mathrm{i}k_x\xi}\,\mathrm{d}\xi \tag{7}$$

A schematic of the different regions of the wavenumber-frequency spectrum Φ_{pp} corresponding to upstream or downstream propagating perturbations of an acoustic or turbulent nature is presented in figure 16.

Finally, the power spectral density of the pressure fluctuations propagating in the upstream direction $S_{pp}^{(-)}$ can be retrieved by integrating Φ_{pp} over $k_x < 0$:

$$S_{pp}^{(-)}(\omega) = \int_{-\infty}^{0} \Phi_{pp}(k_x, \omega)\,\mathrm{d}k_x \tag{8}$$

Downloaded by Christophe Bogey on October 11, 2023 | http://arc.aiaa.org | DOI: 10.2514/6.2023-4188

Downloaded by Christophe Bogey on October 11, 2023 | http://arc.aiaa.org | DOI: 10.2514/6.2023-4188

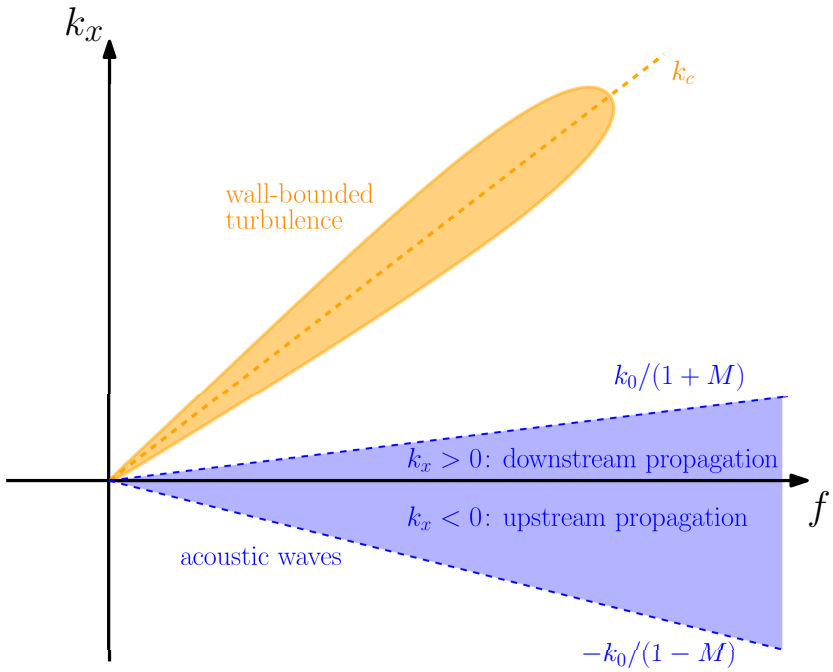

Fig. 16 Regions of the wavenumber-frequency spectrum $\phi_{pp}(k_x, \omega)$ corresponding to upstream or downstream pressure perturbations associated with acoustic waves or the turbulent boundary layer.

The wavenumber-frequency spectrum obtained experimentally for the reference airfoil cascade with a flow Mach number M = 0.34 and for a cascade frontline angle $\beta_c = 34°$ is shown in figure 17. The region corresponding to downstream propagating turbulent boundary layer pressure fluctuations can clearly be identified, as well as the range of wavenumbers corresponding to upstream and downstream propagating acoustic waves. The levels observed for the turbulent boundary layer fluctuations are important, thus they are expected to vastly dominate the raw pressure spectra measured by the microphones.

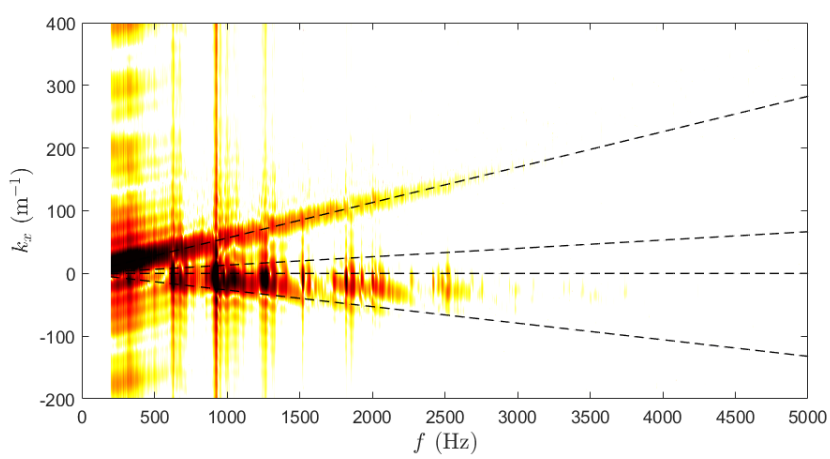

Fig. 17 Wavenumber-frequency spectrum Φ_{pp} for the reference case with a flow Mach number M = 0.34 **and a cascade frontline angle $\beta_c = 34°$.**

This is demonstrated in figure 18 where the raw pressure spectrum or one of the microphones from the linear array is compared to the filtered pressure spectrum $S_{pp}^{(-)}$ containing only the upstream propagating fluctuations, calculated using equation (8). The levels of the filtered spectrum are well below the levels of the raw spectrum over most of the frequency range, but especially at low frequencies, below 600 Hz, and at high frequencies, above 2 kHz. The capability

to separate the upstream propagating components of the pressure fluctuations is thus necessary to compare the acoustic performances of the porous airfoil concept to the reference.

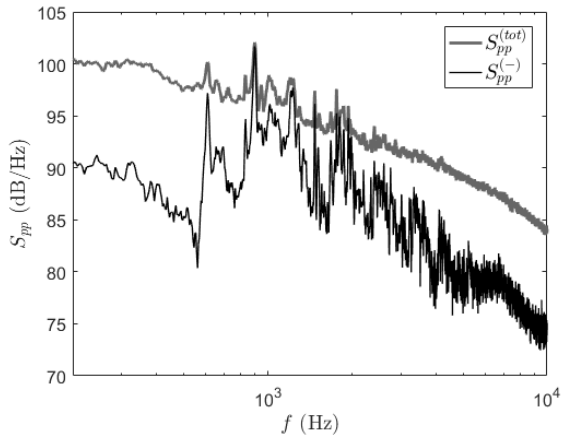

Fig. 18 Comparison between the raw Power Spectral Density of the pressure fluctuations measured for a microphone of the array (gray) and the filtered spectrum accounting only for the upstream propagating waves (black). Reference case with a flow Mach number M = 0.34 **and a cascade frontline angle** $\beta_c = 34°$**.**

The same filtering procedure is applied to the measurements performed with the porous airfoil concept, and the upstream propagating pressure spectra are compared to the reference airfoil cascade in figure 19 for the two Mach numbers M = 0.34 and M = 0.53, and with a cascade frontline angle $\beta_c = 34°$. The observations are slightly different than for the downstream PWL presented in figure 14. The upstream pressure spectra for the porous airfoil concept show lower levels of about 2 to 3 dB for frequencies below 600 Hz. The significant noise increase that was observed downstream around 1 kHz to 2.5 kHz does not appear upstream. Finally, there appear to be some noise reduction above 2.5 kHz, similar to what was observed downstream.

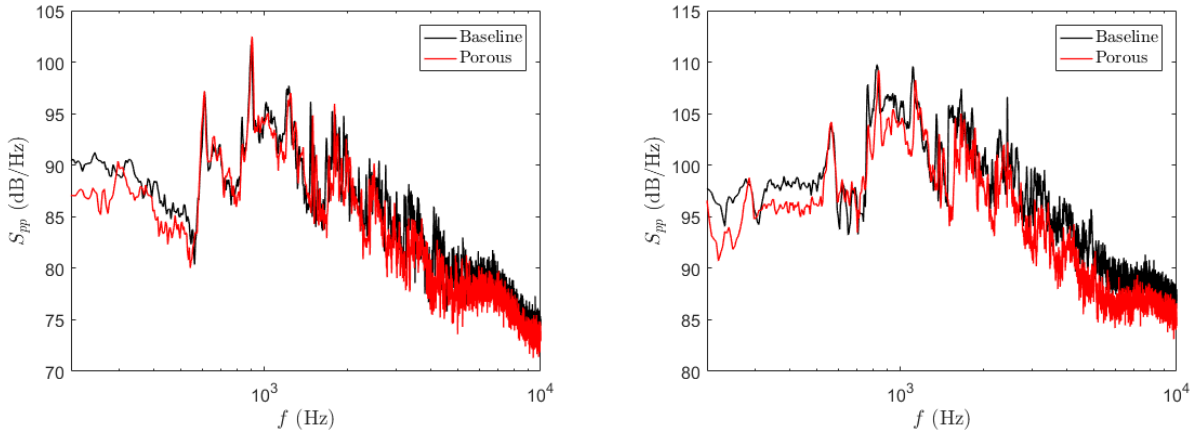

Fig. 19 Power Spectral Density of the pressure fluctuation radiated upstream, measured by the linear microphone array. The cascade frontline angle is $\beta_c = 34°$ **and the upstream flow has a Mach number** M = 0.34 **(left) and** M = 0.53 **(right).**

Overall, the porous airfoil concept developed in this work appear to show some noise reduction at high frequencies, that are unfortunately counterbalanced by an increase of the noise at lower frequencies downstream of the cascade, in the 1 kHz to 2.5 kHz range, where most of the acoustic energy is located. This noise increase is mostly visible downstream of the cascade, but not upstream. The origin of this noise increase is unclear, but may be associated with a possible flow separation for the porous airfoil concept and requires further investigations.

Downloaded by Christophe Bogey on October 11, 2023 | http://arc.aiaa.org | DOI: 10.2514/6.2023-4188

Downloaded by Christophe Bogey on October 11, 2023 | http://arc.aiaa.org | DOI: 10.2514/6.2023-4188

IV. Conclusion

In this paper, the broadband noise resulting from the interaction of a turbulent flow with a rectilinear cascade of airfoils is investigated experimentally in an anechoic wind tunnel. This noise generation mechanism is one of the major source of turbofan engine noise, when the wakes from the fan interact with the OGVs. An airfoil concept consisting in inclusions of porous material in the airfoil and a wiremesh at the surface of the airfoil as been designed and tested in the rectilinear cascade configuration. As the airfoils are loaded and the flow velocities under consideration are up to a Mach number of 0.53, the design of the porous airfoil had to be adapted from previous work for these conditions. Upstream of the cascade, static pressure and hot-wire anemometry measurements were performed and showed the flow to be homogeneous through the test section. The turbulence spectra are consistent with a classical isotropic turbulence model. Hot-wire measurements performed in the wake of the airfoils, near the trailing edge, showed that the wakes for the porous airfoil concept are much wider and have a larger velocity deficit than those of the reference airfoil. The velocity fluctuations in the wake are also much larger for the porous concept. This suggests a possible flow separation for the porous concept, even though the origin of this separation remains unclear at the moment. Acoustic measurements were performed both downstream of the cascade in the far-field, and upstream of the cascade in the duct. The results downstream show a noise reduction with the porous concept above 2.5 kHz, which is counterbalanced by an increase of the noise between 1 kHz and 2.5 kHz, where most of the energy is located in the spectra. This results in an slight overall noise increase at M = 0.34 at all observation angles, and a minimal noise reduction at M = 0.53. Upstream of the cascade, measurements performed with a linear array of microphones aligned in the axial direction are used to separate the noise radiated from the cascade from the turbulent boundary layer pressure fluctuations. The acoustic spectra display a noise reduction above 2.5 kHz similar to the one observed downstream. At lower frequency, no noise increase is visible and a noise reduction is even visible below 600 Hz, contrary to the noise increase observed downstream. Overall, the porous airfoil concept shows a net noise reduction upstream of the cascade, but the noise increase at mid-frequencies downstream of the cascade balances the gains visible at higher frequencies. As the porous airfoil was shown to have much larger and more turbulent wakes, the hypothesis that this noise increase is related to a possible flow separation needs to be investigated further.

Acknowledgments

This work was supported by the Labex CeLyA of the Université de Lyon, operated by the French National Research Agency (ANR-10-LABX-0060/ ANR-16-IDEX-0005).

This project has received funding from the Clean Sky 2 Joint Undertaking (JU) under agreement n°865007. The JU receives support from the European Union's Horizon 2020 research and innovation program and the Clean Sky 2 JU members other than the Union. This publication reflects only the author's view and the JU is not responsible for any use that may be of the information it contains.

References

[1] Envia, E., "Fan Noise Reduction: An Overview," *International Journal of Aeroacoustics*, Vol. 1, No. 1, 2002, pp. 43–64. https://doi.org/10.1260/1475472021502668.

[2] Peake, N., and Parry, A., "Modern Challenges Facing Turbomachinery Aeroacoustics," *Annual Review of Fluid Mechanics*, Vol. 44, 2012, pp. 227–248. https://doi.org/10.1146/annurev-fluid-120710-101231.

[3] Tyler, J., and Sofrin, T., "Axial Flow Compressor Noise Studies," SAE Technical Paper 620532, 1962. https://doi.org/10.4271/620532.

[4] Astley, R., Sugimoto, R., and Mustafi, P., "Computational aero-acoustics for fan duct propagation and radiation. Current status and application to turbofan liner optimisation," *Journal of Sound and Vibration*, Vol. 330, No. 16, 2011, pp. 3832–3845. https://doi.org/10.1016/j.jsv.2011.03.022.

[5] Clair, V., Polacsek, C., Le Garrec, T., Reboul, G., Gruber, M., and Joseph, P., "Experimental and Numerical Investigation of Turbulence-Airfoil Noise Reduction Using Wavy Edges," *AIAA Journal*, Vol. 51, No. 11, 2013, pp. 2695–2713. https://doi.org/10.2514/1.J052394.

[6] Roger, M., Schram, C., and De Santana, L., "Reduction of Airfoil Turbulence-Impingement Noise by Means of Leading-Edge Serrations and/or Porous Material," *19th AIAA/CEAS Aeroacoustics Conference*, 2013. https://doi.org/10.2514/6.2013-2108.

[7] Chaitanya, P., Joseph, P., Narayanan, S., Vanderwel, C., Turner, J., Kim, J.-W., and Ganapathisubramani, B., "Performance and mechanism of sinusoidal leading edge serrations for the reduction of turbulence–aerofoil interaction noise," *Journal of Fluid Mechanics*, Vol. 818, 2017, pp. 435–464. https://doi.org/10.1017/jfm.2017.141.

[8] Bampanis, G., "Airfoil Turbulence-Impingement Noise Reduction by porous cells or wavy leading-edge design," Ph.D. thesis, École Centrale de Lyon, 2021.

[9] Bampanis, G., Roger, M., and Moreau, S., "On a three-dimensional investigation of airfoil turbulence-impingement noise and its reduction by leading-edge tubercles," *Journal of Sound and Vibration*, Vol. 520, 2022. https://doi.org/10.1016/j.jsv.2021.116635.

[10] Chaitanya, P., Joseph, P., Narayanan, S., and Kim, J.-W., "Aerofoil broadband noise reductions through double-wavelength leading edge serrations; a new control concept," *Journal of Fluid Mechanics*, Vol. 855, 2018, pp. 131–151. https://doi.org/10.1017/jfm.2018.620.

[11] Ayton, L., and Chaitanya, P., "An analytical and experimental investigation of aerofoil–turbulence interaction noise for plates with spanwise-varying leading edges," *Journal of Fluid Mechanics*, Vol. 865, 2019, pp. 137–168. https://doi.org/10.1017/jfm.2019.78.

[12] Sarradj, E., and Geyer, T., "Noise Generation by Porous Airfoils," *13th AIAA/CEAS Aeroacoustics Conference*, 2007. https://doi.org/10.2514/6.2007-3719.

[13] Geyer, T., and Sarradj, E., "Trailing Edge Noise of Partially Porous Airfoils," *20th AIAA/CEAS Aeroacoustics Conference*, 2014. https://doi.org/10.2514/6.2014-3039.

[14] Bampanis, G., and Roger, M., "On the Turbulence-Impingement Noise of a NACA-12 Airfoil with Porous Inclusions," *AIAA AVIATION 2020 FORUM*, 2020. https://doi.org/10.2514/6.2020-2577.

[15] Glegg, S., "The Response of a Swept Blade Row to a Three-Dimensional Gust," *Journal of Sound and Vibration*, Vol. 227, No. 1, 1999, p. 29–64. https://doi.org/10.1006/jsvi.1999.2327.

[16] Hanson, D., "Theory for Broadband Noise of Rotor and Stator Cascades With Inhomogeneous Inflow Turbulence Including Effects of Lean and Sweep," NASA Contractor Report 210762, 2001.

[17] Posson, H., Roger, M., and Moreau, S., "On a uniformly valid analytical rectilinear cascade response function," *Journal of Fluid Mechanics*, Vol. 663, 2010, pp. 22–52. https://doi.org/10.1017/S0022112010003368.

[18] Posson, H., Moreau, S., and Roger, M., "On the use of a uniformly valid analytical cascade response function for fan broadband noise predictions," *Journal of Sound and Vibration*, Vol. 329, No. 18, 2010, pp. 3721–3743. https://doi.org/10.1016/j.jsv.2010.03.009.

[19] Bouley, S., François, B., Roger, M., Posson, H., and Moreau, S., "On a two-dimensional mode-matching technique for sound generation and transmission in axial-flow outlet guide vanes," *Journal of Sound and Vibration*, Vol. 403, 2017, pp. 190–213. https://doi.org/10.1016/j.jsv.2017.04.031.

[20] Bouley, S., "Modélisations analytiques du bruit tonal d'interaction rotor/stator par la technique de raccordement modal," Ph.D. thesis, École Centrale de Lyon, 2017.

[21] Girier, L., Roger, M., Bériot, H., Lafitte, A., and Posson, H., "A two-dimensional model of sound transmission through curved and staggered OGV: effect of inter-vane channel mode transitions," *25th AIAA/CEAS Aeroacoustics Conference*, 2019. https://doi.org/10.2514/6.2019-2690.

[22] Girier, L., "Mode-matching techniques for the modeling of rotor-stator wake-interaction tonal noise, with emphasis on the effects of vane camber," Ph.D. thesis, École Centrale de Lyon, 2022.

[23] Smith, E., and Sowers, H., "Cascade Tests of Serrated Leading Edge Blading at High Subsonic Speeds," NASA Contractor Report 2472, 1974.

[24] Sabah, M., "Etude expérimentale du bruit à large bande d'une grille d'aubes. Application au calcul du bruit des soufflantes," Ph.D. thesis, École Centrale de Lyon, 2001.

Downloaded by Christophe Bogey on October 11, 2023 | http://arc.aiaa.org | DOI: 10.2514/6.2023-4188

[25] Posson, H., and Roger, M., "Experimental Validation of a Cascade Response Function for Fan Broadband Noise Predictions," *AIAA Journal*, Vol. 49, No. 9, 2011, pp. 1907–1918. https://doi.org/10.2514/1.J050728.

[26] Mazella, L., Chaitanya, P., Lacagnina, G., Mao, Y., and Joseph, P., "Experimental investigation of the noise control performance of leading edge serrations in a rectilinear cascade," *25th AIAA/CEAS Aeroacoustics Conference*, 2019. https://doi.org/10.2514/6.2019-2472.

Downloaded by Christophe Bogey on October 11, 2023 | http://arc.aiaa.org | DOI: 10.2514/6.2023-4188